STRUCTURAL CONTROL AND HEALTH MONITORING
Struct. Control Health Monit. 2015; **22**:1426–1439
Published online 18 May 2015 in Wiley Online Library (wileyonlinelibrary.com). DOI: 10.1002/stc.1756

An inverse parallel genetic algorithm for the identification of skin/core debonding in honeycomb aluminium panels

V. Meruane*,† and V. delFierro

Department of Mechanical Engineering, Universidad de Chile, Beauchef 851, Santiago, Chile

SUMMARY

Honeycomb sandwich structures are used in a wide variety of applications. Nevertheless, because of manufacturing defects or impact loads, these structures can experience imperfect bonding or debonding between the skin and the honeycomb core. Instances of debonding reduce the bending stiffness of the composite panel, which causes detectable changes in its vibration characteristics. This article presents a new methodology to identify debonded regions in aluminium honeycomb panels that uses an inverse algorithm based on parallel genetic algorithms. The honeycomb panels are modelled with finite elements using a simplified three-layer shell model. The adhesive layer between the skin and core is modelled using linear springs, with reduced rigidity for the debonded sectors. The algorithm is validated using experimental data from an aluminium honeycomb panel containing different damage scenarios. Copyright © 2015 John Wiley & Sons, Ltd.

Received 1 March 2015; Revised 15 April 2015; Accepted 23 April 2015

KEY WORDS: sandwich structures; debonding; honeycomb; parallel genetic algorithms; damage assessment

1. INTRODUCTION

The applications of sandwich structures continue to increase rapidly and range from satellites, aircraft, ships, automobiles, rail cars, wind energy systems and bridge construction, among others [1]. Sandwich panels typically consist of two thin face sheets or skins and a lightweight thicker core, which is sandwiched between two faces to obtain a structure of superior bending stiffness. Nevertheless, because of manufacturing defects or impact loads, these structures can experience imperfect bonding or debonding between the skin and the honeycomb core. Debonding in a sandwich structure may severely degrade its mechanical properties, which can produce a catastrophic failure of the overall structure. Therefore, it is important to detect the presence of debonding at an early stage.

A disadvantage of sandwich structures is that their structural failure, especially in the core, cannot always be detected by traditional nondestructive detection methods. A global technique called vibration-based damage detection has been rapidly expanded over the last few years [2]. The basic idea is that vibration characteristics (natural frequencies, mode shapes, damping, frequency response function, etc.) are functions of the physical properties of the structure. Thus, changes to the material and/or geometric properties due to damage will cause detectable changes in the vibration characteristics. Many studies have demonstrated that vibration characteristics are sensitive to delamination in composite laminates, even if it is located in hidden or internal areas [3,4]. Nevertheless, there have only been a few studies related to the debonding of sandwich structures [5–10]. Jiang *et al.* [5] used a commercial finite element software to investigate the behaviour of debonded honeycomb structures. Their results show that natural frequencies are sensitive indicators to the presence of debonding. Kim and Hwang

*Correspondence to: V. Meruane, Department of Mechanical Engineering, Universidad de Chile, Beauchef 851, Santiago, Chile.
†E-mail: vmeruane@ing.uchile.cl

[6] studied the effect of internal face-layer debonding in the natural frequencies and frequency response functions of a honeycomb beam. Their results reveal that the extent of the debonding plays an important role in determining the natural frequencies and mode shapes of the debonded sandwich beam. Burlayenko *et al.* [7,8] studied the influence of skin/core debonding on the vibrations of honeycomb panels. The authors investigated the influence of the debonding type, size and location on the modal parameters of damaged sandwich panels with different boundary conditions. They concluded that the size of the debonded zone strongly influences the panel modal parameters, reduces the natural frequencies and creates a discontinuity in the mode shapes. This influence is stronger for higher frequency modes. Mohanan *et al.* [9] studied the sensitivity of natural frequencies, mode shapes and modal strain energy to debonds and dents in metallic honeycomb beams. Their results indicate that natural frequencies and mode shapes are sensitive indicators to the presence of damage, but less sensitive in identifying its location and size. However, modal strain energy was more effective in identifying the elements affected by the damage. Shahdin *et al.* [10] presented an experimental study on the effects of impact damage and core-only damage in honeycomb sandwich beams. Their results show that the damage produces a decrease in the natural frequency accompanied by an increase in the damping ratio. Furthermore, the damping ratio is a more sensitive parameter for damage detection than the natural frequencies, although it is much harder to estimate it compared with the natural frequency. Lou *et al.* [11] studied the effects of local damage of the core on the natural frequencies and vibration modes of composite pyramidal truss core sandwich structures by numerical simulation and experimental modal analysis. They concluded that natural frequencies decrease because of the loss stiffness caused by local damage and that vibration modes show local deformation in the damaged region.

Vibration-based damage assessment methods are classified as model based or nonmodel based. Nonmodel-based methods detect damage by comparing the measurements from the undamaged and damaged structures, whereas model-based methods locate and quantify damage by correlating an analytical model with test data from a damaged structure. Additionally, model-based methods are particularly useful for predicting the system response to new loading conditions and/or new system configurations (damage states), allowing damage prognosis [12]. Model-based damage assessment requires the solution of a nonlinear inverse problem, which can be accomplished using supervised learning algorithms as neural networks [12–18] or by global optimisation algorithms [17–26]. Islam and Craig [13] trained a back-propagation neural network with the first five natural frequencies of a composite beam to determine the location and size of any delamination. Natural frequencies were obtained through a modal analysis, which was performed using piezoceramic patches as both sensors and actuators. Back-propagation neural networks were used by Okafor *et al.* [14] to predict delamination size in composite beams based on changes in their natural frequencies. In this case, the delamination is assumed to be at the middle of the beam. The network was able to accurately predict dimensionless delamination sizes between 0.22 and 0.82 but under-predicted delamination sizes below 0.08. A similar approach is used by Valoor and Chandrashekhara [15] to predict delamination locations and sizes in a thick composite beam. They found that the errors were highest for delaminations located near the beam end and that in symmetrical structures, the network can only predict the possible location in each symmetrical segment. Hence, to locate the damage in symmetrical structures, more information, such as mode shapes, is needed. Ishak *et al.* [16] trained a multilayer perceptron network to identify the location, depth and length of delamination in carbon/epoxy laminated composite beams. The network inputs are experimental displacement responses measured with a scanning laser vibrometer. Chakraborty [17] proposed a neural network approach to predict the size, shape and location of delamination in composite panels using natural frequencies. The method was validated using simulated data from a composite panel. The results show that the network works reasonably well when tested with unknown data. Nevertheless, the authors stated that the actual efficacy of the approach can be determined only when the network is trained and tested with experimental data. Su *et al.* [18] compared the efficiency of neural networks and genetic algorithms (GAs) for the evaluation of delaminations in composite beams based on the change in their natural frequencies. The response of the beams is measured using fibre Bragg grating sensors. The authors concluded that both algorithms are able to evaluate the delamination location, size and depth, but neural networks are more stable. Zhang *et al.* [19] examined three different inverse algorithms to predict the location and size of delamination in a composite beam: a direct solution using a graphical method, neural networks and surrogate

DOI: 10.1002/stc

optimisation based on GA. Their results show that the three algorithms can predict the delamination parameters, but neural networks are more sensitive to experimental noise. Zhu *et al.* [20] proposed a GA-based method to identify the location and size of debonding in honeycomb sandwich beams.

There has been significant interest in implementing GAs for damage assessment problems [21–25]. Nevertheless, GAs are inherently slow when they work with complicated or time-consuming objective functions. Parallel genetic algorithms (PGAs) solve this problem; they are particularly easy to implement and provide superior numerical performance [26]. Meruane and Heylen [27] implemented a real-coded parallel GA to detect structural damage. Their results showed that PGAs provided an important increase in the performance compared with the sequential GAs. The parallel algorithm was not only much faster than the sequential algorithm but also able to reach a better solution. This algorithm was later improved [28,29], making each population work with a different crossover. This ensures an effective search with an adequate balance between exploration and exploitation.

This article presents a new methodology to identify debonded regions in aluminium honeycomb panels that uses an inverse algorithm based on parallel GAs. The objective function is based on mode shapes and natural frequencies. It considers a damage penalisation term to avoid false damage detection due to experimental noise or modelling errors. The honeycomb panels are modelled with finite elements using a simplified three-layer shell model. The adhesive layer between the skin and core is modelled using linear springs, with reduced rigidities for the debonded sectors. The algorithm is validated using experimental data from an aluminium honeycomb panel containing different damage scenarios.

2. MODELLING

2.1. Honeycomb panels

Figure 1 shows a scheme for a honeycomb sandwich panel, consisting of two thin face sheets or skins and a honeycomb core, which are bonded together by an adhesive layer. The panel can be modelled by a detailed three-dimensional (3D) finite element model, but the computational effort increases very rapidly as the number of cells increases. Therefore, it is more convenient to develop equivalent simplified model for the honeycomb core to reduce the required computational time. Burton and Noor [30] studied the performance of nine different modelling approaches based on two-dimensional shell theories to predict the static response of sandwich panels. The results are compared with those from a detailed 3D model. Their study showed that the global response can be accurately predicted by discrete three-layer models, predictor–corrector approaches and even first-order shear deformation theory, provided that proper values for the shear correction factors are used. According to Birman and Bert [31], a key factor in the practical application of the first-order shear deformation theory is the determination of the shear correction factor. The analysis presented by these researchers concluded that the shear correction factor should be taken with a value equal to unity for sandwich structures, as a first approximation. The work presented by Burton and Noor [32] showed that continuum layer models for the honeycomb core provide solutions that are close to those calculated by using detailed finite element models. Tanimoto *et al.* [33] used beam elements to model the honeycomb core and the adhesive layer. The proposed model

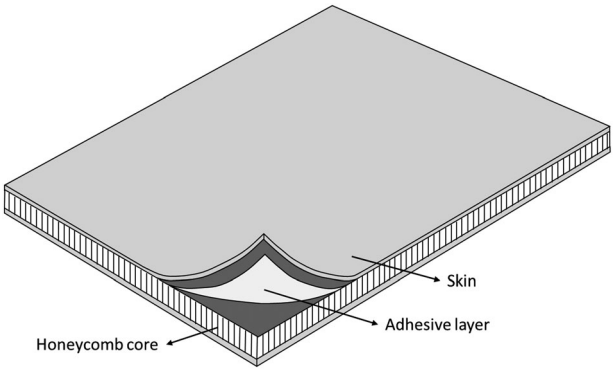

Figure 1. Scheme of a honeycomb sandwich panel.

DOI: 10.1002/stc

was validated by experimental vibration tests. Burlayenko and Sadowski [34] performed an analysis of sandwich plates with hollow and foam-filled honeycomb cores using a commercially available finite element code. The sandwich plates were modelled on the basis of a simplified three-layered continuum model using a mixed shell/solid approach. Consequently, the prediction of the dynamic response of the honeycomb panels can be accomplished by equivalent continuum models.

2.2. Debonding

A debonded region between the skin and core of a honeycomb panel is similar to a delamination in laminated composites. There is a considerable amount of analytical and numerical methods used to model delaminated composite laminates. Della and Shu [35] provide an extensive review of them. The majority of these methods can be categorised into two classes. The first is a region approach where the laminate is divided into sublaminates and continuity conditions are imposed at the junctions, whereas the second is a layer-wise model where delamination is introduced as an embedded layer or as a discontinuity function in the displacement field. On the other hand, modelling vibrations in sandwich structures with debonding is generally accompanied by contact problems between the interfaces of the debonded region [36]. Jiang *et al.* [5] modelled a honeycomb panel as a three-layer structure using 3D solid elements and introduced the debonding between the skin and the core as a noncontacting area. Burlayenko and Sadowski [7,8] modelled the debonded region in honeycomb panels by creating a small gap between the face and the core and by introducing bilinear spring elements between the double nodes in the debonded area. The springs have a stiffness equal to zero in tension and a large value in compression, simulating a contact condition. A piecewise linear model does not predict a unique mode shape as in a linear system, but the mode shape depends on the vibration amplitude.

3. DAMAGE ASSESSMENT ALGORITHM

3.1. Damage parameterisation

To represent the damage, N points are uniformly distributed over the panel, and damage is parameterised by circular-shaped debonded regions centred at some of the N points, as shown in Figure 2. The damage scenario is represented by a vector $\boldsymbol{\beta}=\{\beta_1,\beta_2,..\beta_N\}$, where the value $\beta_i>0$ implies a debonded region with a radius β_i centred at the ith point. Figure 2 illustrates an example of a vector $\boldsymbol{\beta}$ that represents a damage scenario with two debonded regions centred at points r and s.

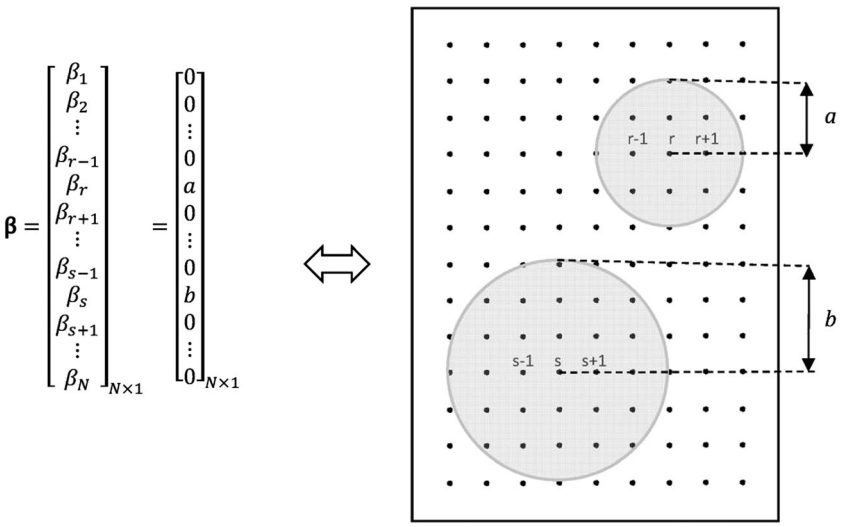

Figure 2. Example of a vector $\boldsymbol{\beta}$ that represents a damage scenario with two debonded regions.

DOI: 10.1002/stc

3.2. Formulation of the optimisation problem

The problem of detecting damage is a constrained nonlinear optimisation problem, where the factors β_i are defined as the updating parameters. The first error function is based on the natural frequency changes due to structural damage and is defined as follows:

$$\boldsymbol{\varepsilon}_{\varpi} = \left(\frac{\boldsymbol{\omega}^D - \boldsymbol{\omega}^U}{\boldsymbol{\omega}^U} \right)^2 \tag{1}$$

where $\boldsymbol{\omega}$ represents a vector containing the natural frequencies and the superscripts D and U refer to damaged and undamaged, respectively. The second error function represents the mode shape changes due to damage and is defined as follows:

$$\boldsymbol{\varepsilon}_{\phi} = \frac{\sum_i \left(\phi_i^D - \phi_i^U \right)^2}{\max\left(\sum_i \left(\phi_i^D - \phi_i^U \right)^2 \right)} \tag{2}$$

where φ_i represents the ith mode shape vector. The vector of the mode shape changes is normalised with respect to its maximum value to reduce the difference between the numerical and experimental results. This difference is because the numerical model does not contain contact conditions and the experimental model does.

The objective function is defined as the normalised sum of the errors plus a damage penalisation term:

$$\begin{aligned} J(\boldsymbol{\beta}) &= W_{\omega} \frac{F_{\omega}(\boldsymbol{\beta})}{F_{\omega,0}} + W_{\varphi} \frac{F_{\varphi}(\boldsymbol{\beta})}{F_{\varphi,0}} + F_D(\boldsymbol{\beta}) \\ F_{\omega}(\boldsymbol{\beta}) &= \left\| \boldsymbol{\varepsilon}_{\omega}^N(\boldsymbol{\beta}) - \boldsymbol{\varepsilon}_{\omega}^E \right\| \\ F_{\varphi}(\boldsymbol{\beta}) &= \left\| \boldsymbol{\varepsilon}_{\varphi}^N(\boldsymbol{\beta}) - \boldsymbol{\varepsilon}_{\varphi}^E \right\| \end{aligned} \tag{3}$$

where $F_{\omega,0,}$ and $F_{\varphi,0}$ refer to the initial values of the sums (when $\beta = 0$), W_{ω} and W_{φ} are weighting factors and the superscripts N and E refer to numerical and experimental, respectively. The variable F_D is a damage penalisation function that helps to avoid false damage detection caused by experimental noise or numerical errors [24]. The damage penalisation function is defined as follows:

$$F_D(\boldsymbol{\beta}) = \gamma \sum_i \delta_i,\ \delta_i = \begin{cases} 1 & \beta_i > 0 \\ 0 & \beta_i = 0 \end{cases} \tag{4}$$

The value of the constant γ depends on the confidence in the numerical model and the experimental data. The following values were used for the constants: $\gamma = 0.05$, $W_{\omega} = 0.5$ and $W_{\varphi} = 1.5$. The optimisation problem is defined as follows:

$$\begin{aligned} &\min && J(\boldsymbol{\beta}) \\ &\text{subject} \quad \text{to} && 0 \le \beta_i \le 0.1 \end{aligned} \tag{5}$$

3.3. Optimisation algorithm

The optimisation problem is particularly challenging, and a robust optimisation algorithm is needed. Based on this, it is proposed to use GAs as an optimisation tool. The GA is a global searching process based on Darwin's principle of natural selection and evolution. A sequential GA consists of three main operations: selection, genetic operations and replacement (Figure 3). The GA starts by creating an initial population. A set of possible solutions, referred to as chromosomes, form the initial population. A sequence of genes that represents the variables of the problem forms each chromosome. The fitness function evaluates the fitness of each chromosome. Next, the algorithm passes the initial population through a selection process. Chromosomes with a higher fitness have a higher probability to survive in the next generation. After the selection process, the chromosomes are randomly paired. Each pair of chromosomes is referred to as parents. The algorithm uses the basic GA operators, crossover and mutation, to reproduce the parents. As a result, it creates new pairs of children. Crossover and mutation are applied randomly with a probability of p_c and p_m, respectively. After the process of selection, genetic operations and replacement, the algorithm evaluates the new population. This process is iterated for a number of generations until a

DOI: 10.1002/stc

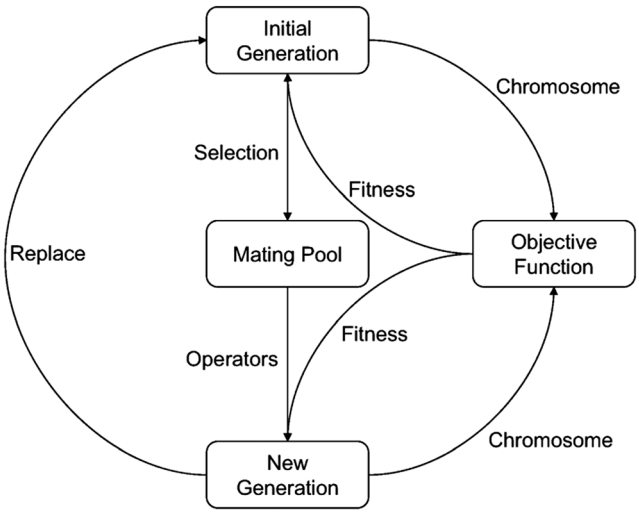

Figure 3. Working principle of a sequential genetic algorithm.

convergence criterion is achieved. The crossover is considered the main search operator. Each crossover technique directs the search in different areas near the parents, and some of them use more exploration (or interpolation) and others more exploitation (or extrapolation). For the algorithm to be successful, there must be an adequate balance between exploration and exploitation. Herrera *et al.* [37] showed that by combining different types of crossovers, the effectiveness of the search can be improved.

The problem with sequential GAs is that they are inherently slow when they work with complicated or time-consuming objective functions. To improve the search speed, PGAs are proposed. PGAs are particularly easy to implement and provide superior numerical performance. Many studies show that with PGAs, the execution time can be reduced by a factor greater than the number of processors used [26]. The basic idea in parallel processing is to divide a large problem into smaller tasks. A group of processors solves these tasks simultaneously. Parallelisation is applied to GAs by different approaches. Three main methods are distinguished: global, migration and diffusion. Migration GAs, also known as multiple population GAs, are the most popular parallel method and potentially the most efficient. In this case, a number of populations are run in parallel. Each population runs a conventional GA individually. These populations exchange their individuals occasionally. This exchange is denominated migration. The separation into subpopulations prevents premature convergence because it allows each population to search in different zones. Meruane and Heylen [27] investigated the advantages of PGAs for structural damage detection problems. They concluded that PGAs always provide an improved and faster search in the solution space when compared with sequential GAs.

Figure 4 illustrates the optimisation algorithm. This algorithm is a multiple population GA with four populations and a neighbourhood migration. Each population runs a sequential GA that from time to time exchanges information with its neighbours (migration). The gene of each chromosome is an updating parameter of the optimisation problem. The GA uses a normalised geometric selection. To ensure an effective search with an adequate balance between exploration and exploitation, each population works with a different crossover: arithmetic crossover, heuristic crossover, BLX-0.5 crossover and uniform crossover. In addition, a crossover function, denoted has extended simple crossover, has been specially developed for this problem and has been incorporated in the four populations. In damage assessment problems, the optimum solution is mostly formed by zeroes and a few values different to zero. The extended simple crossover is particularly useful when the algorithm has found the locations of the damage but not its magnitude. This crossover combines a simple crossover with a linear extrapolation of the parents,

$$\begin{aligned} x' &= \{r_x x_1, r_x x_2, \cdots, r_x x_k, r_y y_{k+1}, \cdots, r_y y_n\} \\ y' &= \{r_y y_1, r_y y_2, \cdots, r_y y_k, r_x x_{k+1}, \cdots, r_x x_n\} \end{aligned} \tag{6}$$

where x and y are the two chromosomes selected for the application of the crossover operator, x' and y' are the two children created by the extended simple crossover and r_x and r_y are uniformly distributed

DOI: 10.1002/stc

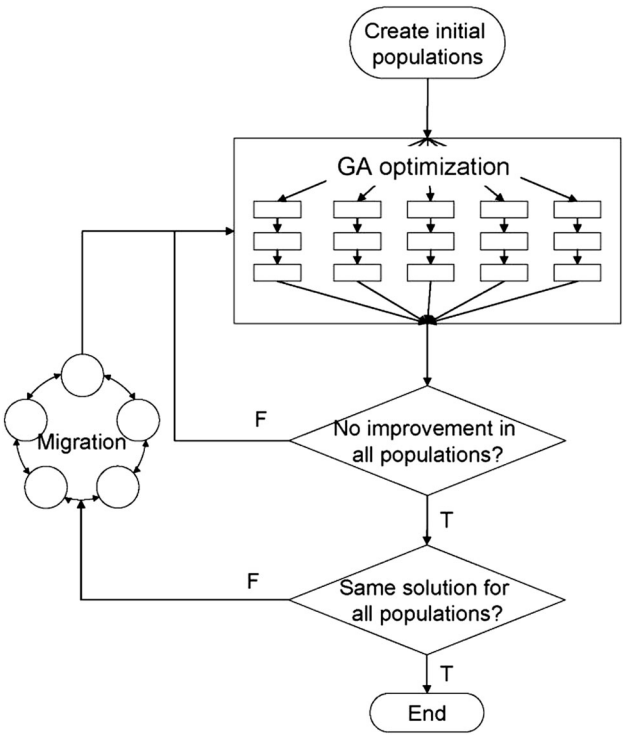

Figure 4. Illustration of the parallel optimisation algorithm. GA, genetic algorithm.

numbers between $(1-\alpha)$ and $(1+\alpha)$. Here, α is set equal to 0.1. If x' or y' is infeasible, that is, one or more of its genes are outside the allowed range, then new random numbers r_x and r_y are generated, and x' and y' are revaluated. To ensure halting, after 10 failures, the children are set equal to the parents.

Each population applies both the boundary and uniform mutations. The population size and the crossover and mutation probabilities are 20 individuals, $p_c = 0.90$ and $p_m = 0.002$, respectively. The migration interval is automatically adjusted. If a population has no improvement after 20 generations, the GA stops and exchanges the individuals with their neighbours. This exchange of individuals is synchronous, that is, the algorithm waits until the four populations are ready to perform the migration. At each migration, each population sends its best individual, whereas its worst individual is replaced by the received individual. Before migration, the best individuals from all populations are compared. If they are all the same, the optimisation is finished.

To create the initial population, a database of mode shapes and natural frequencies associated with single damage scenarios is used. The database contains four debonding diameters for each damage location, resulting in 468 different scenarios. Each scenario in the database is evaluated using the objective function, and the best 20 are selected to form part of the initial population.

4. APPLICATION CASE

The application case corresponds to an aluminium honeycomb panel. The next sections describe the experimental panel, the numerical model and the results of the damage assessment algorithm.

4.1. Experimental panel

The experimental panel consists of a sandwich panels of $0.25 \times 0.35\ m^2$ made of an aluminium honeycomb core bonded to two aluminium skins. The properties of the skin material and the core are summarised in Tables I and II. The skins are bonded to the honeycomb core using an epoxy adhesive that provides a high performance solution to ambient temperature cure bonding of aluminium honeycomb to a wide range of skin materials. Figure 5a shows an aluminium sheet with a layer of epoxy

DOI: 10.1002/stc

Table I. Properties of the skin.

Thickness	0.8 mm
Young's modulus	6.9×10^{10} Pa
Poisson ratio	0.33
Density	2700 kg/m^3

Table II. Properties of the honeycomb core.

Cell size	19.1 mm
Foil thickness	5×10^{-5} m
Thickness	10 mm
Density	20.8 kg/m^3
Compressive strength	0.448 MPa
Shear strength in longitudinal direction (σ_{xy})	0.345 MPa
Shear modulus in longitudinal direction (G_{xy})	89.63 MPa
Shear strength in width direction (σ_{yz})	0.241 MPa
Shear modulus in width direction (G_{yz})	41.37 MPa

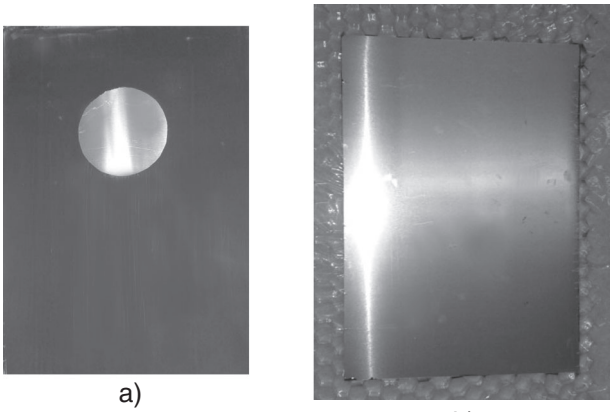

Figure 5. Fabrication of the experimental panel: (a) layer of epoxy adhesive over the skin and (b) vacuum bagging of the panel.

adhesive, and the circular region without adhesive is introduced to simulate debonding. To ensure perfect bonding, the panel is cured using a vacuum bagging system, as shown in Figure 5b.

Figure 6 shows the experimental setup used to simulate a free boundary condition. The honeycomb sandwich panel is suspended by soft elastic bands. The out-of-plane vibration is captured by four miniature piezoelectric accelerometers located in three corners and in the centre of the panel. The panel is excited by an impact hammer at the 117 points described in Figure 6b, resulting in 468 measured frequency response functions.

4.2. Numerical model

In the present study, the honeycomb panels are modelled with finite elements using a simplified three-layer shell model, and the adhesive layer between the skin and core is modelled using linear springs. Because the properties of the skin are known, the attention is focused on modelling the effective properties of the adhesive layer and the core material. The adhesive layer between the skin and core is modelled using linear springs, with reduced rigidity in debonded sectors, as shown in Figure 7.

The numerical model is built in Matlab® using the SDT Structural Dynamics Toolbox (SDTools, Paris, France) [38], and the skins and honeycomb panel are modelled with standard isotropic four-node shell elements. The final model shown in Figure 8 has 10 742 shell and 7242 spring elements.

DOI: 10.1002/stc

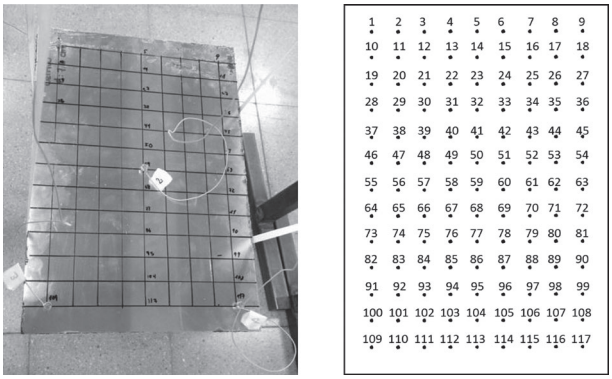

Figure 6. Experimental setup: (a) panel suspended by elastic bands and (b) distribution of measurement points.

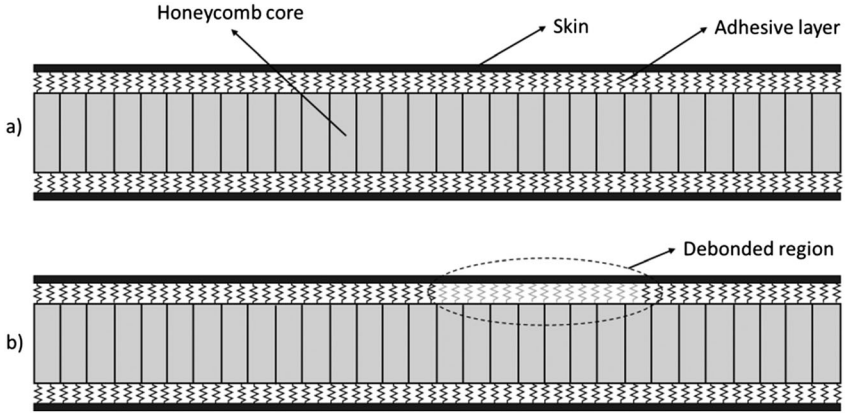

Figure 7. Lateral view of the numerical model: (a) undamaged panel and (b) panel with a debonded region.

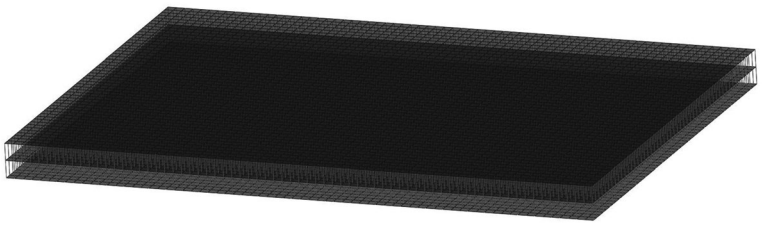

Figure 8. Finite element model of the sandwich panel.

The mechanical properties of the sandwich construction depend upon the adhesives, temperature and pressure used during curing. In addition, the anisotropic nature of the honeycomb core makes testing the sandwich specimens mandatory to determine their properties with accuracy. Here, the mechanical properties of the adhesive layer and the honeycomb core are determined by updating the finite element model with the experimental mode shapes and natural frequencies for both undamaged cases and those with debonding.

Figure 9 shows the first six experimental mode shapes compared with those from the numerical model after updating. The correlation between the numerical and experimental mode shapes is measured by the Modal Assurance Criterion (MAC), a value of 0 indicates no correlation whereas a value of 1 indicates two completely correlated modes. The parameters that were updated in the numerical model are the following: the density and Young's modulus of the skins; the density, bending stiffness and shear correction factor of the core; and the stiffness of the springs representing the adhesive layer.

DOI: 10.1002/stc

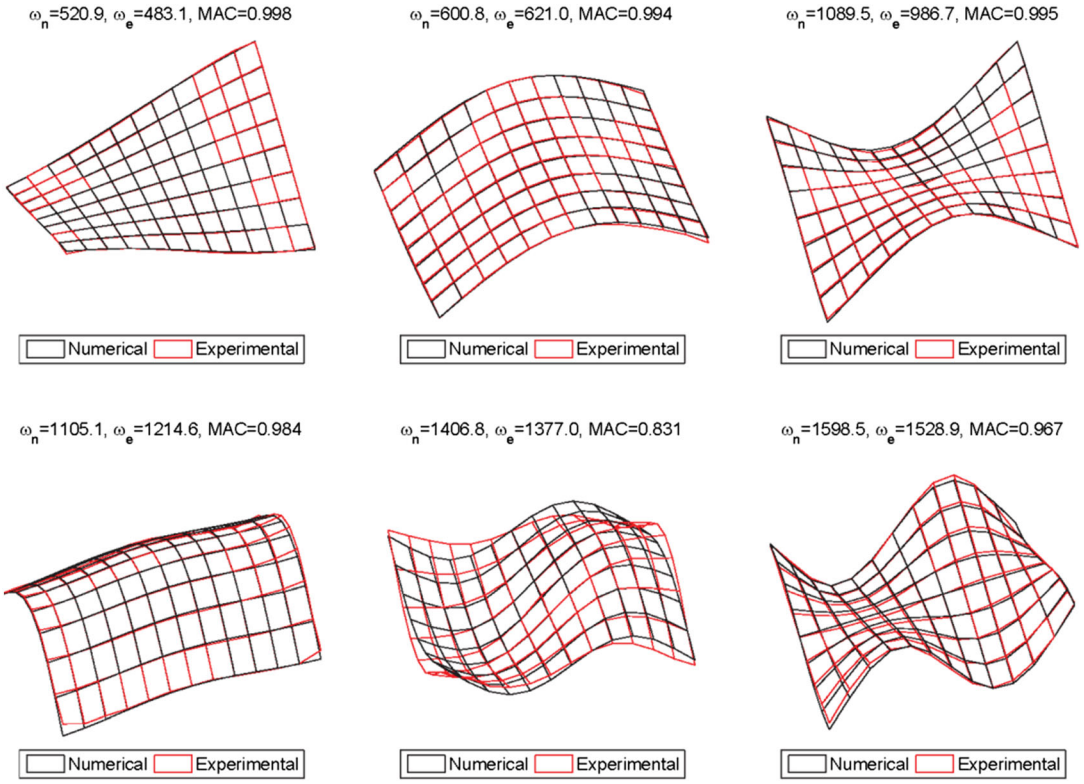

Figure 9. Numerical and experimental undamaged mode shapes.

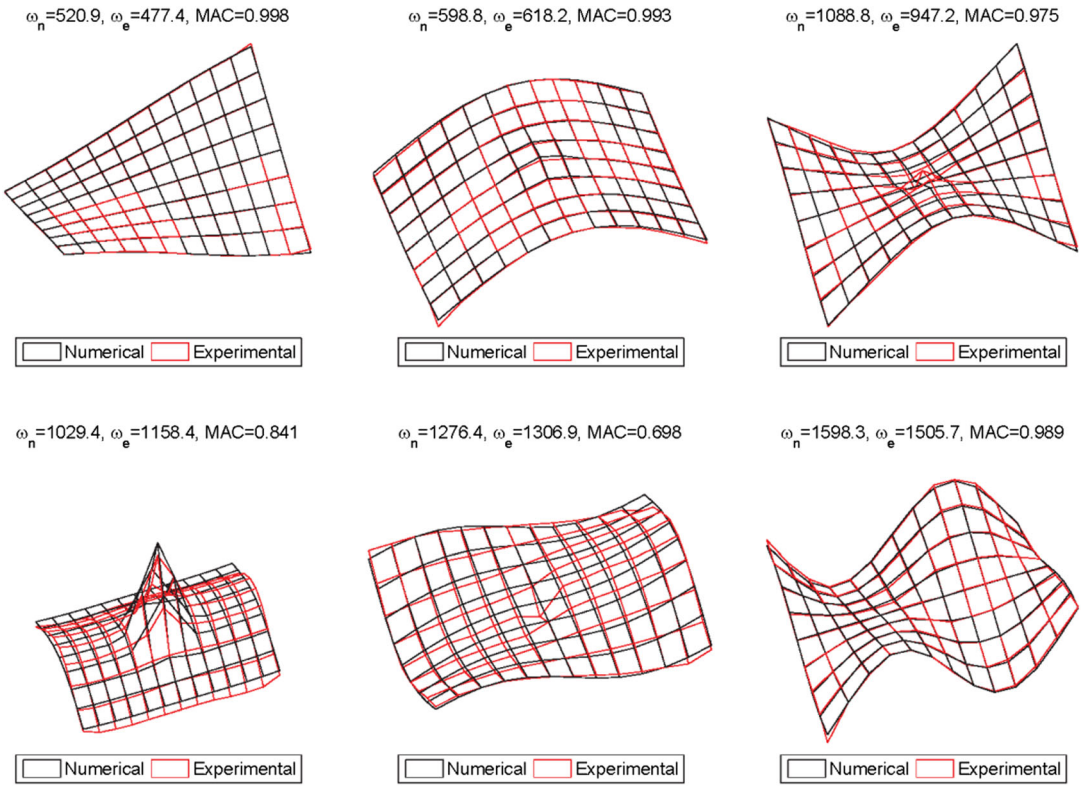

Figure 10. Numerical and experimental mode shapes with a debonded region at the centre of the panel.

DOI: 10.1002/stc

The correlation between the shapes of the numerical and experimental modes is almost perfect for the first three modes with MAC values higher than 0.99. The fifth mode presents the lowest correlation, with a MAC value of 0.83. In this case, the first-order shear approximation may not be sufficient. The maximum difference between the experimental and the numerical natural frequencies is 11%.

Figure 10 presents the correlation between the numerical and experimental modes for the case with a circular debonded region at the centre of the plate. The modes are plotted over the surface of the debonded skin. Here, the numerical model was updated again, considering the spring stiffness in the debonded region as updating parameters. Although the correlation is not as good as in the undamaged case, both the numerical and experimental models show the same behaviour in the presence of damage, which is a reduction in the natural frequencies, and a strong discontinuity at the debonded region for mode 4.

4.3. Results

The algorithm is tested for the three damage scenarios shown in Figure 11. The first case has a debonded region centred at point 59 (the centre of the panel), the second case has a debonded region centred somewhere between points 30, 31, 39 and 40 and the third case has two debonded region centred at points 32 and 86.

To assess damage, debonding is restricted to the skin that is measured during experiments. Figures 12b, 13b and 14b show the damage assessment results for the different damage scenarios. The damage detected is represented as a grey region where each pixel represents a debonded spring. The actual damage introduced into the panel is presented as a circle. In the first case, the centre of

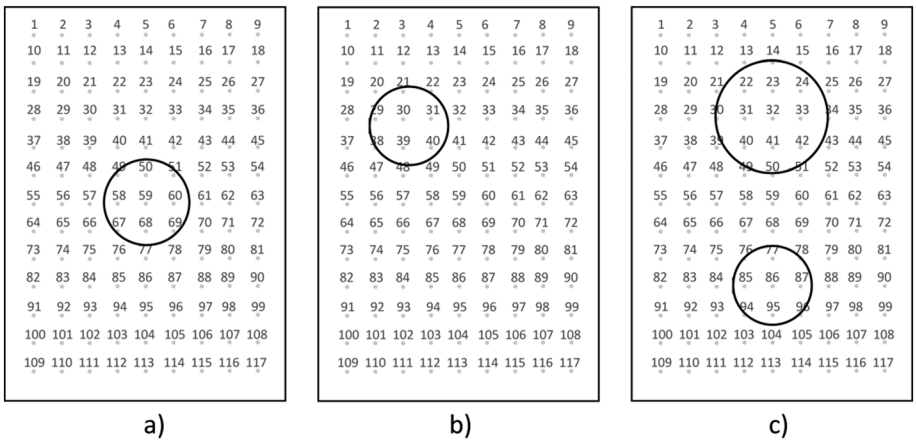

Figure 11. Experimental damage scenarios introduced to the panel; the circles indicate the debonded regions.

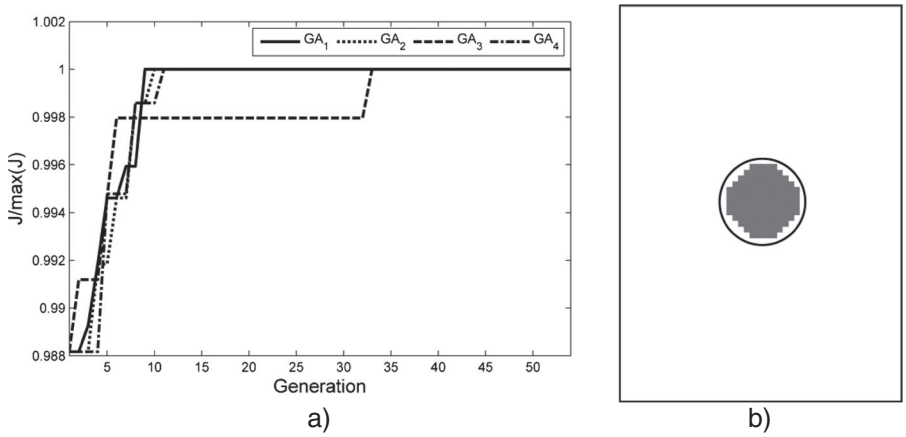

Figure 12. Damage assessment results for the first damage scenario: (a) convergence curves and (b) actual debonded region (circle) versus detected region (grey). GA, genetic algorithm.

DOI: 10.1002/stc

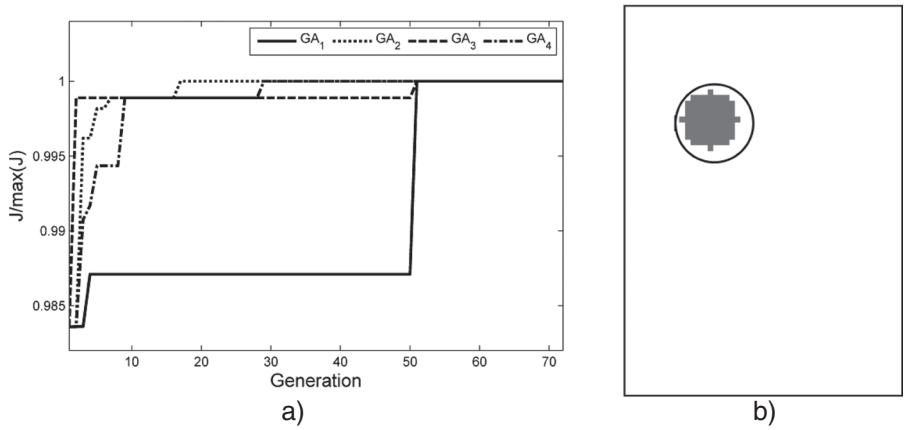

Figure 13. Damage assessment results for the second damage scenario: (a) convergence curves and (b) actual debonded region (circle) versus detected region (grey). GA, genetic algorithm.

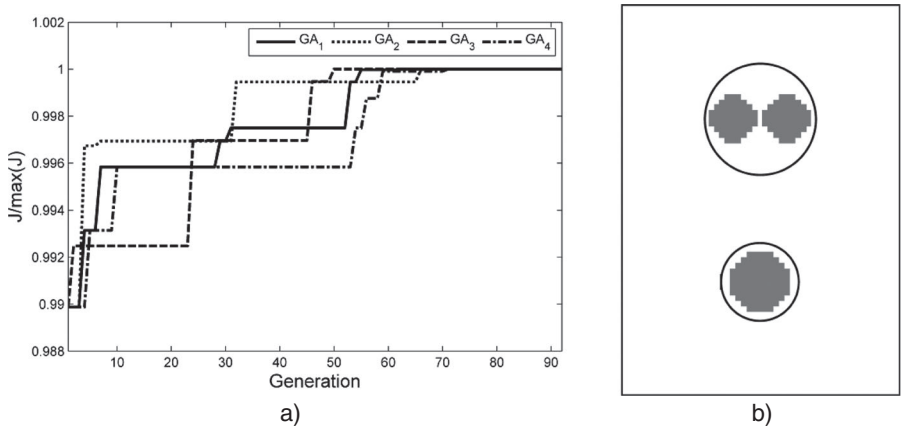

Figure 14. Damage assessment results for the third damage scenario: (a) convergence curves and (b) actual debonded regions (circles) versus detected regions (grey). GA, genetic algorithm.

the experimental damage matches one of the 117 predefined positions. Thus, the algorithm is able to detect the exact position of the debonded region and its magnitude. However, when the actual centre of the damage does not match one of the 117 positions, as in the second case, the algorithm detects the damage at a position that is close to the actual location but not at the exact position. In the third case, at the larger debonded region, the algorithm detected two debonds instead of one.

The convergence curves presented in Figures 12a, 13a and 14a show the evolution of the best individuals in the four populations. The algorithm needed between 60 and 90 generations to reach the optimum. In the first two cases, three populations were able to find a solution close to the optimum before 15 generations, whereas in the third case, the populations reach the optimum after a couple of migrations. This result is explained by the fact that in the third case, there are more possible locations for the debonded regions, and thus, each population may find a different solution.

5. CONCLUSIONS

This article presented a new methodology to identify debonded regions in aluminium honeycomb panels using an inverse algorithm based on PGAs. The algorithm was validated using experimental data from an aluminium honeycomb panel subjected to different damage scenarios.

The honeycomb panels were modelled with finite elements using a simplified three-layer shell model. The adhesive layer between the skin and core was modelled using linear springs, with the

DOI: 10.1002/stc

rigidity reduced in debonded sectors. This numerical model is able to predict with reasonable accuracy the first six modes of the undamaged and damaged panels.

The results show that the algorithm is able to predict the debonding location and size. Hence, global responses such as mode shapes and natural frequencies are suitable indicators of debonding. Further research will focus on the assessment of debonding when the mode shapes are measured at the healthy skin. In addition, further research is needed to study the effects of temperature changes in the debonding assessed.

ACKNOWLEDGEMENTS

Valentina del Fierro was supported by CONICYT grant CONICYT-PCHA/Magíster Nacional/2013-221320691. The authors acknowledge the partial financial support of the Chilean National Fund for Scientific and Technological Development (Fondecyt) under grant no. 11110046.

REFERENCES

1. Vinson JR. Sandwich structures: past, present, and future, in Sandwich Structures 7: Advancing with Sandwich Structures and Materials, Springer, 2005; pp. 3–12.
2. Carden E, Fanning P. Vibration based condition monitoring: a review. *Structural Health Monitoring* 2004; **3**(4):355–377.
3. Zou Y, Tong L, Steven G. Vibration-based model-dependent damage (delamination) identification and health monitoring for composite structures – a review. *Journal of Sound and Vibration* 2000; **230**(2):357–378.
4. Montalvao D, Maia N, Ribeiro A. A review of vibration-based structural health monitoring with special emphasis on composite materials. *The Shock and Vibration Digest* 2006; **38**(4):295.
5. Jiang L, Liew K, Lim M, Low S. Vibratory behaviour of delaminated honeycomb structures: a 3-D finite element modelling. *Computers & Structures* 1995; **55**(5):773–788.
6. Kim H-Y, Hwang W. Effect of debonding on natural frequencies and frequency response functions of honeycomb sandwich beams. *Composite Structures* 2002; **55**(1):51–62.
7. Burlayenko V, Sadowski T. Dynamic behaviour of sandwich plates containing single/multiple debonding. *Computational Materials Science* 2011; **50**(4):1263–1268.
8. Burlayenko VN, Sadowski T. Influence of skin/core debonding on free vibration behavior of foam and honeycomb cored sandwich plates. *International Journal of Non-Linear Mechanics* 2010; **45**(10):959–968.
9. Mohanan A, Pradeep K, Narayanan K. Performance assessment of sandwich structures with debonds and dents. *International Journal of Scientific & Engineering Research* 2013; **4**(5):174–179.
10. Shahdin A, Morlier J, Gourinat Y. Damage monitoring in sandwich beams by modal parameter shifts: a comparative study of burst random and sine dwell vibration testing. *Journal of Sound and Vibration* 2010; **329**(5):566–584.
11. Lou J, Wu L, Ma L, Xiong J, Wang B. Effects of local damage on vibration characteristics of composite pyramidal truss core sandwich structure. *Composites Part B: Engineering* 2014; **62**:73–87.
12. Farrar C, Lieven N. Damage prognosis: the future of structural health monitoring. *Philosophical Transactions of the Royal Society A: Mathematical, Physical and Engineering Sciences* 2007; **365**(1851):623–632.
13. Islam AS, Craig KC. Damage detection in composite structures using piezoelectric materials (and neural net). *Smart Materials and Structures* 1994; **3**:318–328.
14. Okafor AC, Chandrashekhara K, Jiang Y. Delamination prediction in composite beams with built-in piezoelectric devices using modal analysis and neural network. *Smart Materials and Structures* 1996; **5**(3):338–347.
15. Valoor MT, Chandrashekhara K. A thick composite-beam model for delamination prediction by the use of neural networks. *Composites Science and Technology* 2000; **60**(9):1773–1779.
16. Ishak S, Liu G, Shang H, Lim S. Locating and sizing of delamination in composite laminates using computational and experimental methods. *Composites Part B: Engineering* 2001; **32**(4):287–298.
17. Chakraborty D. Artificial neural network based delamination prediction in laminated composites. *Materials & Design* 2005; **26**(1):1–7.
18. Su Z, Ling H-Y, Zhou L-M, Lau K-T, Ye L. Efficiency of genetic algorithms and artificial neural networks for evaluating delamination in composite structures using fibre Bragg grating sensors. *Smart Materials and Structures* 2005; **14**(6):1541–1553.
19. Zhang Z, Shankar K, Ray T, Morozov EV, Tahtali M. Vibration-based inverse algorithms for detection of delamination in composites. *Composite Structures* 2013; **102**:226–236.
20. Zhu K, Chen M, Lu Q, Wang B, Fang D. Debonding detection of honeycomb sandwich structures using frequency response functions. *Journal of Sound and Vibration* 2014; **333**(21):5299–5311.
21. Hao H, Xia Y. Vibration-based damage detection of structures by genetic algorithm. *Journal of Computing in Civil Engineering* 2002; **16**(3):222–229.
22. Rao M, Srinivas J, Murthy B. Damage detection in vibrating bodies using genetic algorithms. *Computers and Structures* 2004; **82**(11-12):963–968.
23. Perera R, Ruiz A, Manzano C. Performance assessment of multicriteria damage identification genetic algorithms. *Computers & Structures* 2009; **87**(1-2):120–127.
24. Meruane V, Heylen W. A hybrid real genetic algorithm to detect structural damage using modal properties. *Mechanical Systems and Signal Processing* 2011; **25**:1559–1573.
25. Jeong M, Choi JH, Koh BH. Performance evaluation of modified genetic and swarm-based optimization algorithms in damage identification problem. *Structural Control and Health Monitoring* 2013; **20**(6):878–889.
26. Punch W. How effective are multiple populations in genetic programming. *Genetic Programming* 1998; **98**:308–313.

DOI: 10.1002/stc

27. Meruane V, Heylen W. Damage detection with parallel genetic algorithms and operational modes. *Structural Health Monitoring* 2010; **9**(6):481–496.
28. Meruane V, Heylen W. Structural damage assessment with antiresonances versus mode shapes using parallel genetic algorithms. *Structural Control & Health Monitoring* 2011; **18**(8):825–839.
29. Meruane V, Heylen W. Structural damage assessment under varying temperature conditions. *Structural Health Monitoring* 2012; **11**(3):345–357.
30. Burton WS, Noor AK. Assessment of computational models for sandwich panels and shells. *Computer Methods in Applied Mechanics and Engineering* 1995; **124**(1):125–151.
31. Birman V, Bert CW. On the choice of shear correction factor in sandwich structures. *Journal of Sandwich Structures and Materials* 2002; **4**(1):83–95.
32. Burton W, Noor A. Assessment of continuum models for sandwich panel honeycomb cores. *Computer Methods in Applied Mechanics and Engineering* 1997; **145**(3):341–360.
33. Tanimoto Y, Nishiwaki T, Shiomi T, Maekawa Z. A numerical modeling for eigenvibration analysis of honeycomb sandwich panels. *Composite Interfaces* 2001; **8**(6):393–402.
34. Burlayenko VN, Sadowski T. Analysis of structural performance of sandwich plates with foam-filled aluminum hexagonal honeycomb core. *Computational Materials Science* 2009; **45**(3):658–662.
35. Della CN, Shu D. Vibration of delaminated composite laminates: a review. *Applied Mechanics Reviews* 2007; **60**(1):1–20.
36. Müller I. Clapping in delaminated sandwich-beams due to forced oscillations. *Computational Mechanics* 2007; **39**(2):113–126.
37. Herrera F, Lozano M, Sanchez A. Hybrid crossover operators for real-coded genetic algorithms: an experimental study. *Soft Computing – A Fusion of Foundations, Methodologies and Applications* 2005; **9**(4):280–298.
38. Balmes E, Jean-Philippe Bianchi J-ML. Structural dynamics toolbox user's guide, Version 6.1, SDTools, 2010.

DOI: 10.1002/stc